

Article

A Metaheuristic Approach to Analyze the Techno-Economical Impact of Energy Storage Systems on Grid-Connected Microgrid Systems Adapting Load-Shifting Policies

Bishwajit Dey ^{1,*}, Senthil Krishnamurthy ¹, Nande Fose ¹, Mukovhe Ratshitanga ¹ and Prathaban Moodley ²

¹ Department of Electrical, Electronics and Computer Engineering, Center for Intelligent Systems and Emerging Technologies, Cape Peninsula University of Technology, Bellville 7535, South Africa; krishnamurthys@cput.ac.za (S.K.); nandetillax@gmail.com (N.F.); ratshitangam@cput.ac.za (M.R.)

² South African National Energy Development Institute (SANEDI), Upper Grayston Office Park, Sandton 2146, South Africa

* Correspondence: sonu.aec2007@gmail.com

Abstract: Battery energy storage systems (BESSs) and plug-in hybrid electric vehicles (PHEVs) are essential for microgrid operations to be financially viable. PHEVs can serve as mobile storage devices, storing excess energy during times of low demand and delivering it during times of high demand. By offering reliable on-site energy storage, BESSs improve cost efficiency by allowing the microgrid to store cheap, off-peak electricity and release it when prices increase. To minimize generation costs and alleviate grid stress during periods of high demand, load-shifting policies shift inelastic loads to off-peak hours when energy prices are lower. When combined, these tactics support dependable, affordable, and effective microgrid management. A recently developed RIME algorithm is used as the optimization tool to reduce the total operating cost (TOC) of an MG system for three cases and three situations. The cases emphasize a modified load demand style influenced by the optimal load-shifting method (OLSM) and order characteristics load-shifting policy (OCLSP), whereas the situations refer to the inclusion of ESS in the MG system. The TOC decreased from \$2624 without ESS to \$2611 and \$2331 with PHEVs and BESSs, respectively. These costs were further reduced to \$1192, \$1162, and \$1147, respectively, when OLSM was implemented to restructure the base load demand. Additionally, a balance between a minimal TOC and carbon emission was obtained when an OLSM-based load demand model was used with BESSs. The RIME algorithm outperformed many recently developed algorithms and is consistent and robust, yielding better quality solutions.

Keywords: BESSs; PHEV; OLSM; microgrid; RIME optimization



Academic Editor: Mohan Lal Kolhe

Received: 13 November 2024

Revised: 25 December 2024

Accepted: 27 December 2024

Published: 31 December 2024

Citation: Dey, B.; Krishnamurthy, S.; Fose, N.; Ratshitanga, M.; Moodley, P. A Metaheuristic Approach to Analyze the Techno-Economical Impact of Energy Storage Systems on Grid-Connected Microgrid Systems Adapting Load-Shifting Policies. *Processes* **2025**, *13*, 65. <https://doi.org/10.3390/pr13010065>

Copyright: © 2024 by the authors. Licensee MDPI, Basel, Switzerland. This article is an open access article distributed under the terms and conditions of the Creative Commons Attribution (CC BY) license (<https://creativecommons.org/licenses/by/4.0/>).

1. Introduction

Recent years have seen a worldwide grid revolution driven by the increased participation of renewable integrated distributed generation (DG), the adoption of government policies, and crucially, the modernization of grid technology. The concept of a microgrid has been established to enhance the advantages of the electrical utility system by facilitating energy integration. A hybrid microgrid, capable of operating in either an off-grid or a grid-connected mode, is formed by integrating several distributed generators (DGs) with diverse loads that operate near an electrical border. The microgrids may be linked to either low- or medium-voltage distribution networks. For rural communities, an off-grid microgrid system is more economically advantageous than a grid-connected operation. The operation of a grid-connected microgrid as an off-grid may be achieved by isolating

the microgrid from the main grid during maintenance or times of significant fault. The off-grid systems provide many benefits like the reliable provision of electricity to the end user, proper coordination with local communities for the auxiliary power system, and the efficient utilization of renewable energy-based distributed devices.

1.1. Literature Review

For the effective management of a microgrid, using the concept of multi-agents, a new coordinated dispatch model has been given [1]. Here, transparency in the data among the components of the microgrid alleviates the operational issues so the coordinated management of the load, battery, and power sources can be achieved. A model-based online optimum control approach [2] can be used to achieve optimal scheduling choices for energy management systems (EMSs). A unique two-stage distributionally robust model is proposed [3] for the efficient model and management of islanded microgrid systems, a subject that has been largely overlooked. To address the variable characteristics of renewable energy, the project strategy and operational decisions are optimized by reducing both expenditure and operating expenses. The optimization of battery performance [4] operations in both stand-alone and grid-connected DC microgrids (MGs) with photo voltaic generators operating at the maximum power point has been investigated. Study paper [5] chose several grid involvements and evaluation methodologies, including the impact of valve point loading and the unpredictability of wind energy, to increase the intricacy and applicability of the study. The author in [6] proposed a robust methodological approach for developing optimal patterns of hybrid microgrid systems (HMGs). A new hierarchical model for dynamic scheduling to wind photovoltaic storage microgrid was proposed in the research article [7], which used colored Petri nets (CPNs). This technique facilitates thorough oversight of information flow and optimizes energy management.

It evaluates the impact of variable price elasticity on increasing operation costs for decentralized producing units and the pricing for utility electricity transactions. In [8], an efficient economic dispatch approach has been considered for a grid-connected microgrid. A hybrid intelligence technique was formulated for the development of a DSM methodology [9] that minimizes the generation costs and reduces the pollution caused by DERs inside a grid-connected LV microgrid system. In research article [10], bi-level optimization was utilized for the minimization of operational costs. This work utilized a novel hybrid swarm intelligence algorithm, which has been shown to be successful in solving a wide range of optimization difficulties to optimize power systems.

Research paper [11] communicates a stochastic expert methodology dedicated to cost reduction in overall operations for designing the optimal energy management strategy of a grid-connected low-voltage microgrid, accounting for both the charging effect of plug-in hybrid electric vehicles and the optimum sizing of the battery energy storage systems. Article [12] provides the ability to study both the internal and the external markets in order to allow the successful participation of MGs in energy trading, including energy exchanges between MGs and the utility grid (UG). Energy pricing was analyzed as two competing objectives: a microgrid's aspiration for increased economic efficiency by lowering the cost of purchases and dependency on utility grids and the distribution network operator's goal to maximize profit from the applied market. Paper [13]'s necessities are concerned with the objective of minimizing an MG system's operating costs via proper energy management (EM) whilst integrating DG, BSS, and PHEVs, and appropriate EM also determines optimal BSS size. An energy consumption modeling approach for large-scale consumers was created in study [14]. This approach included the examination of renewable energy resources, microturbines, energy storage strategy, and bilateral contracts centered on power exchange. The demand-side management, reduction in the expense of energy storage, and related

expertise would primarily benefit larger firms. Study [15] investigated the optimization of the multi-timescale management of CMES at the power and energy stages, respecting the interplay between the source and load. Article [16] discusses a reduction in operating costs and emissions for a daily schedule together with incorporation of load demand, market pricing, and different renewable energy sources for generating electricity. To address the complex optimization problem, this paper introduces the slime mold algorithm. Three scenarios are then tested for SMA, with both operating cost reduction and emission savings taken into account as two objectives. In [17], the authors discuss a novel IDSM approach for an energy system that combines a non-cooperative game framework with multi-energy estimating practices. In study [18], the adjusted loads on both user and system sides were used by the devices to formulate a model for generalized energy storage (GES). The comprehensive design integrates electric vehicles, batteries, flexible resources, and a control system for temperature regulation. Two modifications were implemented in the slime mold algorithm (SMA) to enhance its capabilities in exploration and exploitation, as detailed in the publication [19]. A position update mechanism using sine and cosine functions and opposition theory was utilized.

Conversely, the intricacy of the isolated microgrid may be understood by including different types of loads such as electric vehicles (EVs) during different charging modes, which can result in energy imbalance in off-grid systems. Batteries are likely indispensable for future power transmission networks as very critical components. Considering its time-dependent energy storage properties and higher power capacity, this technology has attracted interest in many common applications, including electric vehicles (EVs).

To minimize operational expenses and harmful emissions, this paper [20] proposes an optimal management system for microgrids that integrate electric vehicles with distributed power production. The research paper [21] presents a novel viewpoint on the vehicle to grid (V2G) technology inside a microgrid, which integrates a demand-side response (DSR) algorithm. An analysis of the microgrid control system deployed on a physical testing platform is presented. A sustainable approach for the management of the allocation and scheduling of solar distributed generation (SDG), public fast-charging stations (PFCSs), and battery energy storage systems (BESSs) has been proposed by the researchers [22]. An optimal solution is achieved by reducing the energy loss, voltage deviation index, investment, and operation maintenance expenses of SDG, PFCS, and BES and considering battery degradation.

According to study analysis [23], the radial distribution network is integrated with the road network to optimize the positioning of electric vehicle charging stations (EVCSs). The weightage of a site is determined by the charging demand, which is entirely influenced by factors such as residential areas, traffic intersections, and the strategic placement of supermarkets. To optimize the integration of electric vehicles (EVs) in the targeted area while minimizing the financial investment required for their installation, it is crucial to minimize energy loss, decrease voltage deviations in the power network, and reduce land costs.

To manage the increase in future demand, the researchers in paper [24] proposed a reliable and durable approach to determine the capacity and placement of fast-charging electric vehicle (EV) stations, as well as the best-planned multistage extension of the distribution network. Research article [25] presents an efficient energy management (EM) approach for a hybrid AC-DC microgrid (HMG). It is divided into two phases: forecasting and scheduling. The validity and performance of the suggested framework are tested by using IEEE standard test systems. The ITLBO algorithm is also used to determine the generating cost and the optimal power dispatch of the HMG. A new approach to the boost in energy management and scheduling within a microgrid is proposed in article [26]. An en-

hanced gradient-based optimization algorithm, IGBO, is used to optimize the production of renewable energy resources with the aim of minimizing the operational cost. In article [27], a detailed technoeconomic analysis is carried out to study the impact of price-dependent demand response programs on optimum scheduling of microgrids in nonlinear and linear load models. The DSM strategy in research paper [9] utilizes the hybrid intelligence technique, proposing an approximate solution between minimized generation cost and pollutant emissions within a five-unit distribution system and an LV microgrid system. Study [28] presents comprehensive techno-economic analysis for the clean and efficient functioning of two differentiated grid-connected low voltage (LV) microgrid (MG) systems.

1.2. Novel Contribution Bridging the Research Gap from Exhaustive Literature Survey

- i. Restructuring the base load demand model according to two different types of loads shifting policies thereafter comparing the MG system efficiency parameters such as reduction in ultimate load and enhancement in load factors.
- ii. Implementing the latest RIME algorithm to evaluate the minimum total operating cost (TOC) of the MG system without energy storage systems (ESSs), with PHEVs, and with battery energy storage systems (BESSs).
- iii. Reinvestigating point (ii) for various load demand models as mentioned in point (i) above.
- iv. Obtaining a trade-off between minimal TOC and pollutants emitted for the MG system with PHEVs and BESSs.
- v. Conducting a performance analysis of RIME algorithms with other recently developed metaheuristic algorithms.

1.3. Arrangement of the Paper

In Section 2, we define the objective functions and constraints of the problem, which include the mathematical modeling of BESSs and OLSM. The optimization method is described in Section 3. The results and discussion, including the validation of the methodology and quality assessment of all results, are presented in Section 4. Section 5 concludes by summarizing important findings and limitations that guide the way forward in furthering the research endeavor.

2. Objective Function

2.1. Formulation of Objective Function

An expression for the cost function of a microgrid (OF1) linked to the main grid at t hours is given by Equation (1) [5], where X_a represents the cost coefficient of the ath unit, $P_{a,t}$ represents the power output of the ath at time t , $S_{grid,t}$ represents the electricity tariff, and $P_{grid,t}$ represents the power output of the main grid. The quantity of pollution-emitting gases, namely carbon dioxide, discharged into the environment by traditional fossil fuel-based units (OF2) may be expressed as Equation (2) [5], where Q_a represents the quantity of pollution-emitting gases by unit a , and $Q_{grid,t}$ represents the quantity of pollution-emitting gases by the main grid. To attain equilibrium between two separate objective functions with specific objectives, Equations (1) and (2) can be merged into Equation (3) [5]. The variable can range from 0 to 1. $OF1_{min}$ and $OF2_{min}$ represent the optimal values derived from minimizing Equations (1) and (2), respectively. $OF3$ represents the balanced economic emission dispatch measure. The values of $OF1_{max}$ and $OF2_{max}$ are derived by replacing the optimum values obtained from minimizing Equations (1) and (2). The optimal values of $OF1$ and $OF2$ may be derived by appropriately taking into account the ideal parameters for $OF1_{min}$ and $OF2_{min}$ in the two equations. Several constraints on the operation may be represented as Equations (4)–(7) [5], where LD_t is the load demand at time t , and

$U_{res,t}$ is the power output of the renewable energy source (RES) at time t . Estimating the projected production of renewable energy sources (RESs) requires taking into account their intermittent nature.

$$OF1 = \sum_t^{24} \sum_{a=1}^n \left(X_a \times P_{a,t} + S_{grid,t} \times P_{grid,t} \right) \quad (1)$$

$$OF2 = \sum_t^{24} \sum_{a=1}^n \left(Q_a \times P_{a,t} + Q_{grid,t} \times P_{grid,t} \right) \quad (2)$$

$$OF3 = \gamma \times \left[\frac{OF1 - OF1_{min}}{OF1_{max} - OF1_{min}} \right] + (1 - \gamma) \times \left[\frac{OF2 - OF2_{min}}{OF2_{max} - OF2_{min}} \right] \quad (3)$$

$$\sum_{a=1}^n P_{a,t} = LD_t \quad (4)$$

$$\sum_{a=1}^n P_{a,t} + U_{res,t} + P_{grid,t} = LD_t \quad (5)$$

$$P_{a,min} \leq P_a \leq P_{a,max} \quad (6)$$

$$P_{grid,min} \leq P_{grid} \leq P_{grid,max} \quad (7)$$

2.2. Wind Power Output Modeling

The power output of a wind turbine is contingent upon wind velocity. Given that the speed of the wind is stochastic inconsistent, the power output of wind turbines is thus an unpredictable quantity. The power output of the wind turbine is dependent on the speed of the wind (v_w) [29]:

$$P_W = \begin{cases} 0, & v_w \leq v_{ci} \\ m + nv_w, & v_{ci} \leq v_w \leq v_r \\ P_r, & v_r \leq v_w \leq v_{co} \\ 0, & v_w \leq v_{co} \end{cases} \quad (8)$$

$$m = P_r v_{ci} / (v_{ci} - v_r), n = P_r / (v_r - v_{ci}) \quad (9)$$

The behavior of wind speed may be modeled using the Weibull distribution function, which is expressed as follows [29]:

$$f(v_w) = 1 - \exp\left(-\left(\frac{v_{ci}}{c}\right)^k\right) + \exp\left(-\left(\frac{v_{co}}{c}\right)^k\right), \text{ where } v_w \leq v_{ci}, v_w > v_{co} \quad (10)$$

$$f(v_w) = 1 - \exp\left(-\left(\frac{v_{ci}}{c}\right)^k\right) - \exp\left(-\left(\frac{v_{co}}{c}\right)^k\right), \text{ where } v_r < v_w \leq v_{co} \quad (11)$$

The PDF for the WT output can be expressed as follows:

$$f(P_W) = \frac{k}{c} \left(\frac{P_{WT} - m}{nc} \right)^{k-1} \exp\left[-\left(\frac{P_{WT} - m}{nc}\right)^k\right], \text{ where } v_{ci} < v_w \leq v_r \quad (12)$$

$$f(P_W = 0) = 1 - \exp\left(-\left(\frac{v_{ci}}{c}\right)^k\right) + \exp\left(-\left(\frac{v_{co}}{c}\right)^k\right), \text{ where } v_w \leq v_{ci}, v_w > v_{co} \quad (13)$$

$$f(P_W = P) = \exp\left(-\left(\frac{v_{ci}}{c}\right)^k\right) - \exp\left(-\left(\frac{v_{co}}{c}\right)^k\right), \text{ where } v_r < v_w \leq v_{co} \quad (14)$$

$$k = \left(\frac{\sigma_w}{\bar{v}_w} \right)^{-1.086} \quad (15)$$

$$c = \frac{\bar{v}_w}{\Gamma\left(\frac{1}{k} + 1\right)} \quad (16)$$

2.3. PV Solar Power Output Modeling

The PV power output depends on the solar irradiance (s_i). Meanwhile, solar irradiation itself is a stochastic unpredictable; the power of photovoltaic systems is, therefore, an undefined quantity. The stochastic characteristics of solar irradiation are represented in Equation (17) by employing a beta distribution function [29]:

$$f(S_i) = \frac{\Gamma(\alpha_s + \beta_s)}{\Gamma(\alpha_s)\Gamma(\beta_s)} S_i^{\alpha_s - 1} (1 - S_i)^{\beta_s - 1}, \quad 0 \leq S_i \leq 1, \alpha_s \geq 0, \beta_s \geq 0$$

$$= 0, \text{ Otherwise} \quad (17)$$

α_s and β_s are derived with the help of the standard deviation (σ_s) and the mean (μ_s) of solar irradiation as follows [29]:

$$\alpha_s = \mu_s \left(\frac{(1 - \mu_s)\mu_s}{\sigma_s} - 1 \right) \quad (18)$$

$$\beta_s = (1 - \mu_s) \left(\frac{(1 - \mu_s)\mu_s}{\sigma_s} - 1 \right) \quad (19)$$

$$f(P_{PV}) = \frac{\Gamma(\alpha_s + \beta_s)}{\Gamma(\alpha_s)\Gamma(\beta_s)} \left(\frac{P_{PV}}{P_{PV,max}} \right)^{\alpha_s - 1} \left(1 - \frac{P_{PV}}{P_{PV,max}} \right)^{\beta_s - 1}$$

$$= 0, \text{ Otherwise} \quad (20)$$

2.4. Formulation of PHEVs Charging and Discharging

Plug-in hybrid electric vehicles (PHEVs) have a limited battery capacity. Consequently, they need charging stations that provide expedited access. As a result, charging stations are established in public and residential zones to mitigate this problem. The charging demand for PHEVs is random because it depends on several factors. The proposed regulated and smart charging method effectively deals with the need of charging PHEVs to reduce peak load, as illustrated in the following calculation [30]:

$$\text{Min} \left(\frac{C_{Grid,t}}{\alpha_{PHEV}} \times \rho_{PHEV}(t) \right) \quad (21)$$

The coefficient α_{PHEV} in use currently is the feasibility of supplying PHEVs at a suitable point of charge. $\rho_{PHEV}(t)$ is the average kW PHEV charging demand per hour.

The method of controlled charging [30]:

$$\sum_{t=T_1}^{T_2} \rho_{PHEV}(t) = E \quad (22)$$

The sign “ E ” denotes the total energy need of PHEVs quantified in kilowatt-hours (kWh). The letter “ t ” denotes the time index. If the duration of T_1 to T_2 lies during the off-peak period, it is known as the controlled charging of PHEVs. If the duration of T_1 to T_2 lies during the period when the electricity price, $C_{Grid,t}$, is lower, it is known as the smart charging mechanism of PHEVs.

The state of charge (SOC) of the battery in a PHEV must be within its minimum limits when the PHEV arrives at the charging station and the maximum limit during the PHEV's departure from the charging station, as mentioned in Equation (23) [30].

$$SOC^{T_1} = SOC_{\min}; SOC^{T_2} = SOC_{\max} \quad (23)$$

The value of $\rho PHEV(t)$ is defined to lie between the lowest and maximum limits of $\rho PHEV$ and may be articulated as follows [30]:

$$\rho PHEV, \min \leq \rho PHEV(t) \leq \rho PHEV, \max \quad (24)$$

$\rho PHEV, \min$ and $\rho PHEV, \max$ denote the minimum and maximum hourly demand for PHEV in kilowatts, respectively.

2.5. Battery Energy Storage Systems

The types of operation modes for BESSs include charging, discharging, and idle modes. This means BESSs can exploit off-peak hours for charging and peak hours for discharge and seize low and high energy costs for charging and discharge, respectively. It takes advantage of the lower need for load as well as cheaper electricity during times of storage, but the stored energy is deployed during peak demand times to serve load needs. Equation (25) describes the charging or discharging power of the battery energy storage system under maximum charging and discharging constraints. In this way, it can charge at the peak solar power availabilities of the day and discharge at the peak loads of the day [31].

$$\begin{aligned} 0 &\leq u_{B,m}^t P_{B-,m}^t \leq P_{B-,m}^{\max}; \\ 0 &\leq v_{B,m}^t P_{B+,m}^t \leq P_{B+,m}^t; m \in \vartheta_K; t \in T \end{aligned} \quad (25)$$

$$u_{B,m}^t + v_{B,m}^t \leq 1; m \in \vartheta_K; t \in T \quad (26)$$

$$SOC_{B,m}^t = SOC_{B,m}^{t-1} + \frac{\left(\eta_B^- P_{B-,m}^t - \frac{P_{B+,m}^t}{\eta_B^+} \right)}{E_{B,m}^C} \Delta t; \quad (27)$$

$$m \in \vartheta_K; t \in T$$

$$SOC_{B,m}^{\min} \leq SOC_{B,m}^t \leq SOC_{B,m}^{\max}; SOC_{B,m}^{\text{in}} = SOC_{B,m}^f \quad (28)$$

$$m \in \vartheta_K; t \in T$$

The binary variables, $u_{B,m}^t$ and $v_{B,m}^t$, inhibit the concurrent charging and discharging action in Equation (26). The battery's state of charge may be assessed using Equation (27), which quantifies the amount of stored energy in the battery. $SOC_{B,m}^t$ is limited by positive and negative limits to prevent battery degradation and maximize the life cycle of service. The battery operating limit associated with the beginning and end state of charge of the BESSs is provided in Equation (28) [31].

2.6. Optimal Load-Shifting Method (OLSM)

OLSM is an efficient economic mechanism that entails relocating flexible loads to times when utility bills reduce their rates [32]. The use of OLSM systems may provide many advantages for the electrical system. Cost reduction, load factor improvement, and peak demand management may be achieved without affecting the total load demand. An in-depth examination of the OLSM approach and its mathematical models for optimization is presented in this part. The load-shifting technology is the most often used among the six available methods. The load-shifting method integrates the approaches of peak cutting

and valley filling. Utilizing changeable loads at the end of consumers enables the efficient transmission of electricity demand. The use of the load-shifting approach allows for a rational modification in energy usage by transferring regulated loads from periods of high to low energy availability. In Figure 1, several methods used for load shaping are shown.

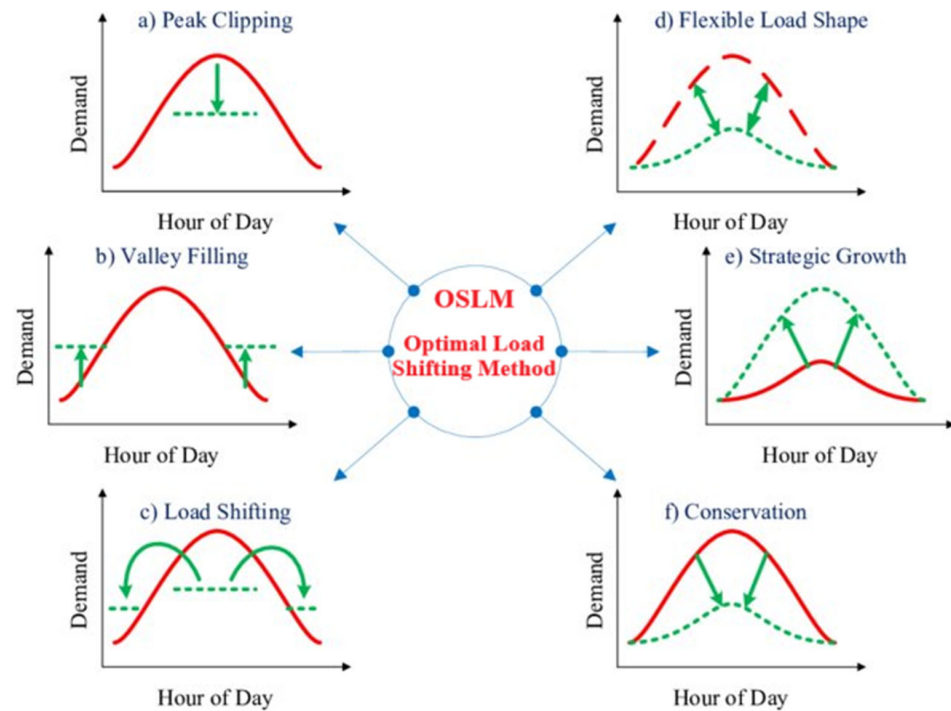


Figure 1. OLSM implementation methods [32].

The fundamental components of load modeling using OLSM are as follows:

Step 1. Specify the varying demand across a time interval of T hours.

Step 2. Provide the utility's time of use (TOU) rate for T hours.

Step 3. When shiftable loads are not expressly indicated, modify the OLSM participation rate.

Step 4. Identify the loads that are capable of being moved and those that are not, considering the level of involvement in OLSM. For example, for each time index, $x\%$, OLSM shows that $x\%$ of demand may be moved, while the remaining is a non-shiftable, load which is $(100 - x)\%$. The optimization of the load shape is achieved by taking into account the elastic load demand.

Step 5. Obtain the minimum and maximum values, along with the total of the inelastic load demand. Special attention should be given to the need to optimize the elastic load.

Step 6. Minimize employing Equation (29), using the optimization technique [32],

$$\text{Minimize } \sum_{t=1}^T \left[c_C^t \times (elst_{load} \text{ at } t^{th} \text{ hour} + enelst_{load} \text{ at } t^{th} \text{ hour}) \right] \quad (29)$$

where

$$0 \leq elst_{load} \text{ at } t^{th} \text{ hour} \leq \text{maximum elastic load}$$

$$\sum_{t=1}^T P_{load}^t = \sum_{t=1}^T \left(elst_{load} \text{ at } t^{th} \text{ hour} + enelst_{load} \text{ at } t^{th} \text{ hour} \right)$$

Step 7. Obtain the modified load model developed from the OLSM by adding the non-shiftable load at all time indices to the optimum forecasted values of the demand for the shiftable load.

The OLSM level is established by the proportion of a regulated or elastic load relative to the overall load demand. The OLSM level may range from 0% to 100%, depending upon the elastic load. The anticipated load demand is the load demand that results in minimal operational expenses. To achieve the projected load, it is anticipated that the total load need is either elastic or regulated. Despite its lack of reality, it is used to evaluate the robustness of a work or plan.

3. RIME Optimization Algorithm

Rime ice occurs when water vapor in the atmosphere collects, shrinks, and freezes at a certain temperature onto various surfaces like tree branches [33]. Figure 2 illustrates that sections of this area face annual landscape changes where rime ice is developed due to specific climatic features and geography.



Figure 2. (a,b) Hard-rime puncturing [33].

In this part, the impacts of the freezing coefficient, wind speed, growth time, and cross-sectional areas of linked materials are investigated, and the growth process of every single rime strip is simulated. RIME has four different stages of operation: initializing the RIME mass, formulating a policy for soft rime exploration, executing a process for a hard rime puncture, and lastly, refining the greedy selection procedure. The initial phase involves setting up the entire rime population R . As per Equation (30) [33], the population consists of n rime agents S_i , each having d rime particles x_{ij} , where j runs from 1 up to an ordinal number for the rime particle, and i generally denotes the ordinal number of the rime representative.

$$R = \begin{bmatrix} x_{11} & x_{12} & \cdots & x_{1j} \\ x_{21} & x_{22} & \cdots & x_{2j} \\ \vdots & \vdots & \ddots & \vdots \\ x_{i1} & x_{i2} & \cdots & x_{ij} \end{bmatrix} \quad (30)$$

As is clear from Equation (31) [33], the position of the rime particles is obtained by temporarily modeling the process of condensation of rime particles and subsequently converting the rime particles keen on soft rime agents, which satisfy the five moving criteria for rime particles.

$$R_{ij}^{new} = R_{best,j} + r_1 \cos \theta \cdot \beta \cdot (h \cdot (Ub_{ij} - Lb_{ij}) + Lb_{ij}), \quad r_2 < E \quad (31)$$

Here, i and j signify the j th element of the i th rime agent, whereas R_{ij}^{new} is used to represent the new position of the updated particle. R is the rime population, and $R_{best,j}$ is the j th particle of the optimal rime agent. The value r_1 is a stochastic variable within the range

$(-1, 1)$ and, along with $\cos\theta$, influences the trajectory of particle movement depending upon the number of repetitions, as shown in Equation (32). The environmental variable ensures that an algorithm will converge because it monitors the number of iterations in order to find the repeated external influences as indicated by Equation (33) [33]. The adhesion coefficient “ h ” is a stochastic variable in the range from 0 to 1. The distance between the centers of two rime particles is controlled by this “ h ”.

$$\theta = \pi \times \frac{t}{10 \times T} \quad (32)$$

In this context, “ t ” denotes the latest number of iterations, whereas “ T ” signifies the algorithm’s maximum iteration capacity.

$$\beta = 1 - \left\lceil \frac{w \times t}{T} \right\rceil / w \quad (33)$$

Within the context of this scenario, the step function serves as the mathematical simulation, β signifies rounding, and the conventional choice of w is 5 to determine the maximum number of segments in the step function. UBij and LBij represent the upper and lower limits of the escape place, correspondingly, and are managed to restrict the successful region of element migration. This is accomplished by referencing Equation (31) [33]. As per Equation (34), the quantity E , indicative of the degree of connection, directly influences the possibility of condensation of an agent. This quantity escalates with an increase in the number of repetitions.

$$E = \sqrt{(t/T)} \quad (34)$$

r_2 is a stochastic number in the period [33] that works with E , which oversees managing particle condensation. It is an indicator of whether the locations of the particles have or have not been changed.

The formation processes of hard rime are more direct and uniform with extreme gale conditions than soft rime. The process of condensation and transformation of a rime particle into solid rime indicates an initiation point of the puncturing phenomena and signifies a procedure for puncturing the solid rime. This can be applied to revise the algorithm amongst agents, thus allowing algorithmic particles to exchange and enhance both the rate of convergence of the algorithm as well as its ability to escape local optima. Figure 3 illustrates the puncture phenomenon, and Equation (35) gives the formula for particle replacement.

$$R_{ij}^{new} = R_{best,j}, r_3 < F^{normr}(S_i) \quad (35)$$

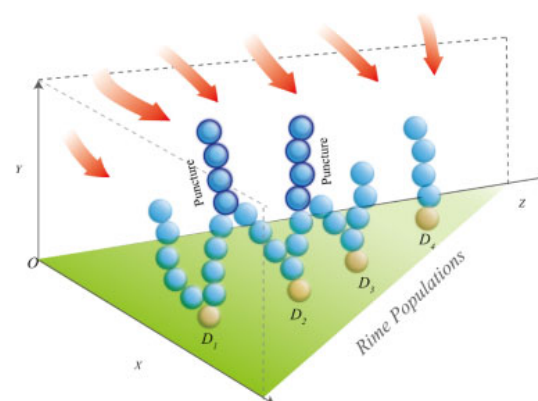


Figure 3. Hard rime puncturing [33].

4. Results and Discussion

4.1. Preliminary Elaboration for the Test System, Software Environment Studied in Varying Situations and Cases

The MG features three microturbines, a fuel cell, two wind turbines, and a solar power system, all integrated with the grid. Three cases and three situations, as mentioned in Table 1 were studied wherein minimum fuel and electricity costs, carbon emissions, and a trade-off between minimal cost and emission were obtained using the RIME algorithm. A single-line diagram of the same is shown in Figure A1 of the Appendix A section. The limits of the fuel cell, microturbine, and grid along with the cost and carbon emission constant are tabulated in Table 2. The electricity tariff and load demand of the system are depicted in Figure 4. Figure 5 represents the likely hourly productivity of RES in a day considering hostile weather conditions. Tables 3 and 4 display the permissible operating constants of the PHEVs and BESSs, respectively. The study is executed in MATLAB 2017a environment in a laptop with an Intel i5 processor and 8GB RAM. The recently developed RIME algorithm [33] is used as the optimization tool for the work due to its simplicity of execution and swift and robust nature. The population size was 80, and the stopping criteria were 1000 iterations.

Table 1. Studying cases and situations.

Cases	Situations
1	Without energy storage systems
2	With PHEVs
3	With BESSs

Table 2. DER parameters associated with the MG system.

DER	Lower Bound (kW) [25]	Higher Bound (kW) [25]	Bids (€/kW) [25]	Carbon Emission (gm/kW)
FC	9	60	0.294	0.1033
MT1	9	60	0.269	0.7620
MT2	50	250	0.215	0.7620
MT3	65	250	0.275	0.7826
Utility	−80	80	Figure 4	0.5546

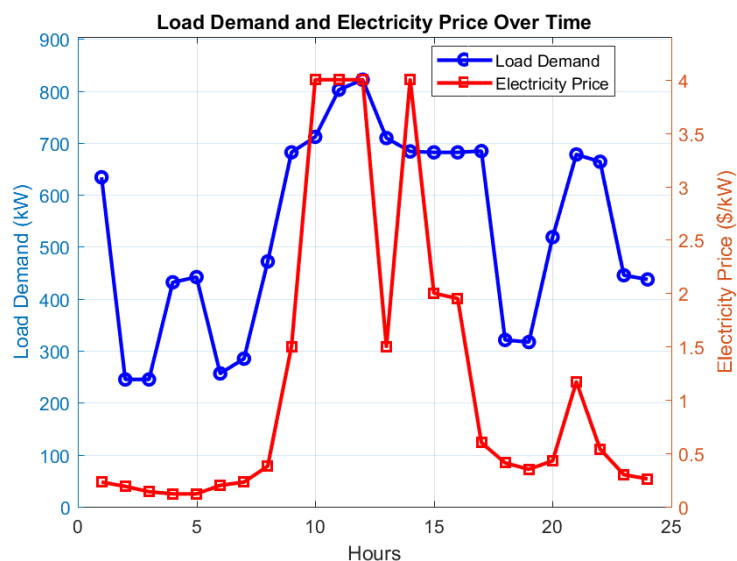


Figure 4. Load demand and electricity price for the subject MG system [25].

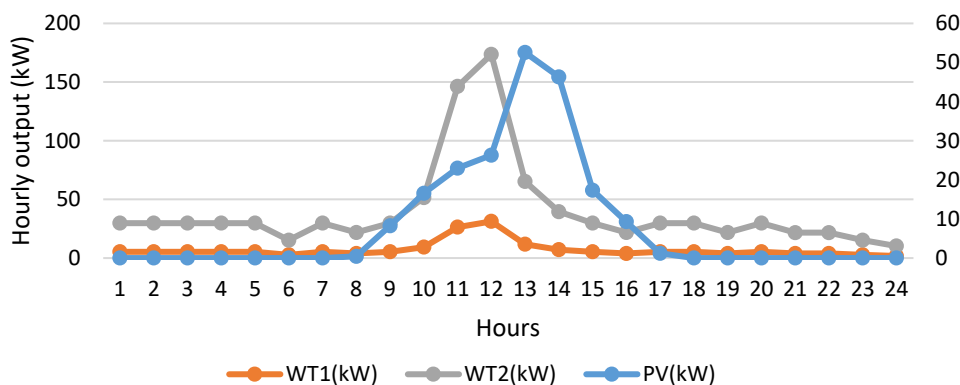


Figure 5. Forecasted power output from renewable energy sources [25].

Table 3. Description of PHEV parameters.

Parameters	Numerical Values
Default Arrival Time	0900 HRS
Default Departure Time	1700 HRS
Arrival SOC	20%
Departure SOC	90%
Battery Capacity	47.4 kWh
Charging/Discharging Power	±12.5 kW
Charging/Discharging Rate	Same as Electricity Price (Figure 2)

Table 4. Description of BESS parameters.

Parameters	Numerical Values
Battery Capacity (kWh)	100
Initial SOC	50% of Battery Capacity
SOC _{min}	10% of Battery Capacity
SOC _{max}	90% of Battery Capacity
Charging/Discharging Efficiency	90%
Charging/Discharging Power	±20 kW
Charging/Discharging Rate	0.38 €ct/kW

4.2. Case Studies for Different Situations

Case 1: For the base load profile, the fuel and electricity costs were minimized for all three situations using the RIME algorithm. The minimum fuel and electricity costs were \$2624, \$2611, and \$2331 for Situations 1, 2, and 3, respectively. Due to the involvement of energy storage systems, the TOC is seen to be decreasing in the latter two situations. However, PHEVs serve as an additional source of energy storage, which charges and discharges exchanging power as per the G2V and V2G strategy during its limited time in the charging station (from the 9th to the 17th hour in this work). BESSs, on the other hand, are a part of the MG system that contributes to the total load demand and is operational throughout the day. Hence, the TOC is lesser for Situation 3 compared to Situation 2. Figures 6–8 show the hourly output of DERs without ESS, with PHEV, and with BESSs, respectively. PHEVs can be seen operating between the 9th and 17th hour, whereas BESSs operate throughout the day. Figure 9 shows that the SOC constraints, as mentioned in Tables 3 and 4, were maintained by the PHEVs and BESSs, respectively.

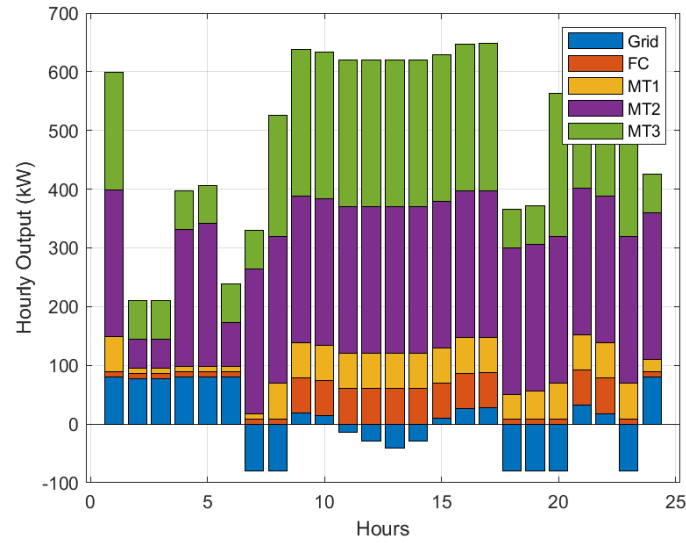


Figure 6. Hourly output of DERs for minimum TOC in Case 1, Situation 1.

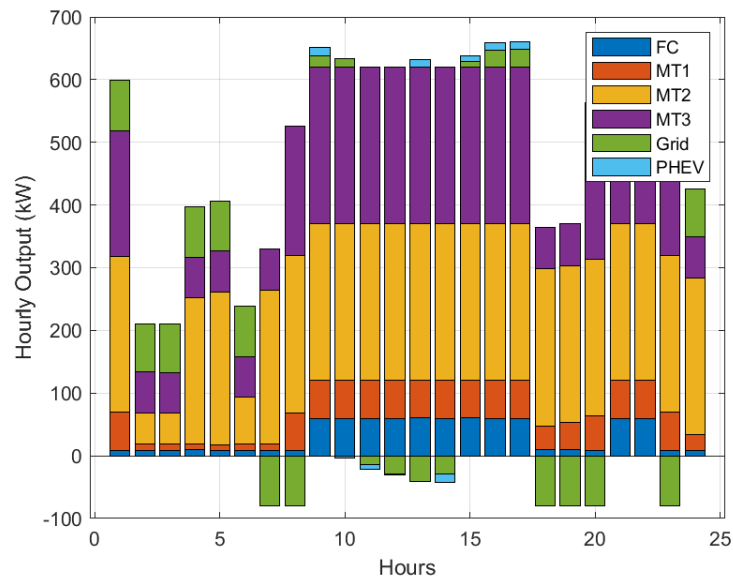


Figure 7. Hourly output of DERs for minimum TOC in Case 1, Situation 2.

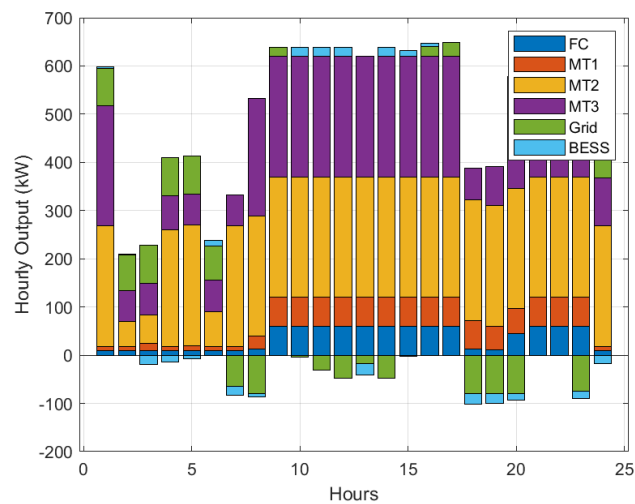


Figure 8. Hourly output of DERs for minimum TOC in Case 1, Situation 3.

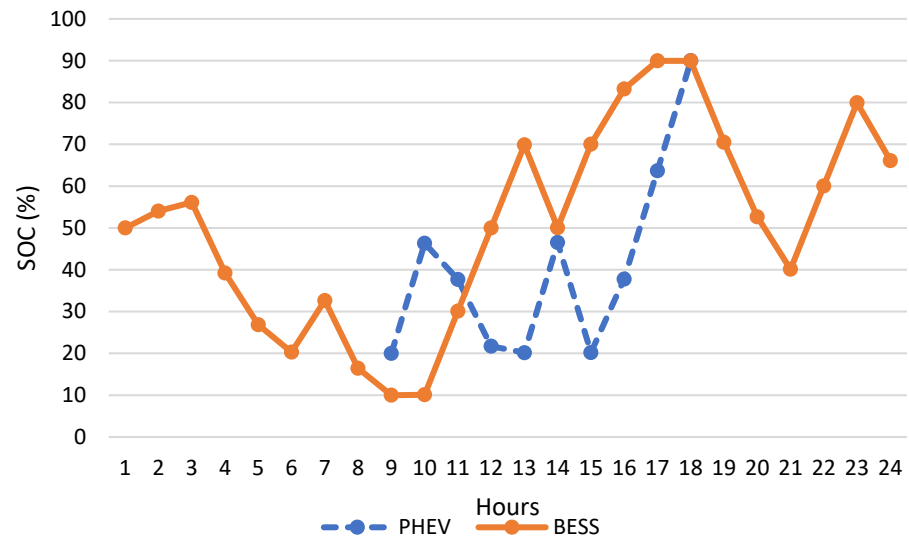


Figure 9. SOC for PHEV and BESSs in Case 1.

Case 2: A recently developed OCLSP [32] employs straightforward procedures to restructure the predicted load demand and create four distinct and independent modified load demands based on the ordered arrangement of the base load, in contrast to the other DSM and DR policies, which use laborious and complicated methodologies and even specialized optimization tools to shift or curtail load demand. The nicest thing about OCLSP is that, although there are observable increases in the load factor (PAR) and a decrease in the system’s peak demand, the overall and average load demand at the end of the day stays the same. Assuming that 30% of the loads are elastic in nature, OCLSP was implemented to obtain four different load profiles, as shown in Figure 10. Table 5 shows a 5% decrement in the peak load from 821 kW to 776 kW. There was a significant improvement in the load factor as well. The TOC was found to be lower for the descending load profile among the four for all the situations examined, as depicted in Table 5. Figures 11 and 12 show the hourly output of DERs when the TOC was \$2039 and \$1758 for Situations 2 and 3, respectively.

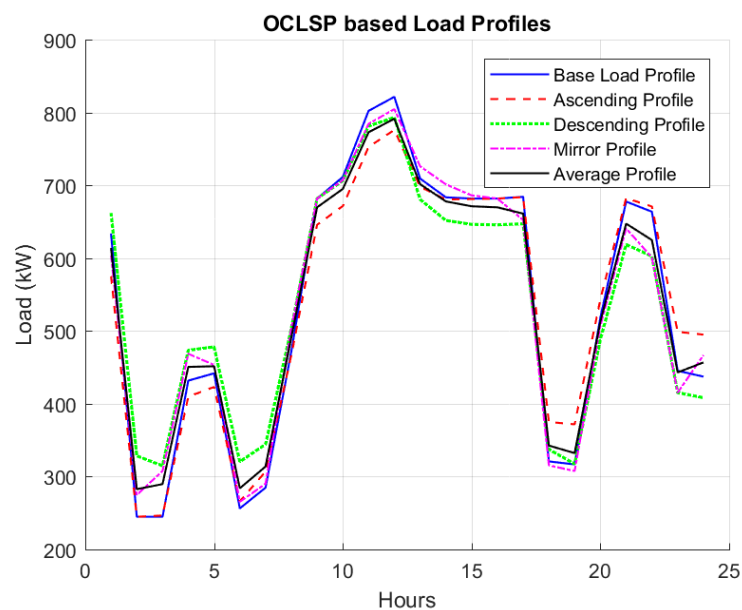


Figure 10. OCLSP-based load demand curves.

Table 5. Load profile characteristics for Case 2 and corresponding TOC.

	Base Load	Ascending Profile	Descending Profile	Mirror Profile	Average Profile
Total Load (kW)	12,846.92	12,846.92	12,846.92	12,846.92	12,846.92
Average Load (kW)	535.2883	535.2883	535.2883	535.2883	535.2883
Peak Load (kW)	821.5	776.0793	793.3375	804.6625	791.3598
Load Factor	0.6516	0.6894	0.6747	0.6653	0.6764
TOC Situation 1 (\$)	2624	2058	2050	2505	2203
TOC Situation 2 (\$)	2611	2045	2039	2493	2190
TOC Situation 3 (\$)	2331	1795	1758	2214	1908

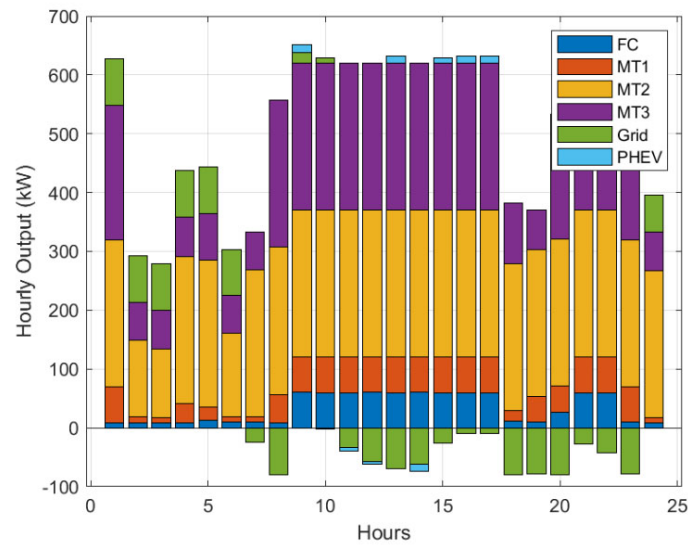


Figure 11. Hourly output of DERs for minimum TOC in Case 2, Situation 2.

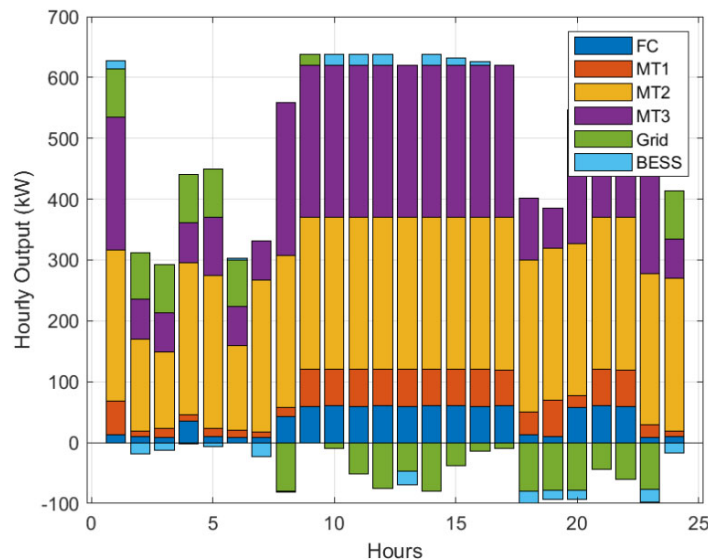


Figure 12. Hourly output of DERs for minimum TOC in Case 2, Situation 3.

Case 3: Assuming that 30% of the load every hour is shiftable in nature, OLSM was performed as mentioned in detail in Section 2.6 above. OLSM is an optimization-based load-shifting method that is entirely dependent on the hourly electricity market price set by the utility. Hence, Case 3 is a bi-level optimization framework wherein the optimal load-shifting is performed in the first level by the RIME algorithm, and thereafter, the

minimization of TOC is performed. Table 6 shows improvement both in TOC and the system performance of the MG. A 16% decline in the peak load was observed, which also resulted in a 19% improvement in the load factor of the MG system when the load demand was modified using OLSM. Figure 13 shows the base load demand and the modified load demand as per OLSM. There was also a major decline, in the range of 50–58%, in the TOC for all three scenarios, as seen in Table 6. Figures 14–16 depict the hourly outputs of DERs when the minimum TOC was obtained using the RIME algorithm for Situations 1, 2, and 3, respectively.

Table 6. Load profile characteristics for Case 3 and corresponding TOC.

Parameters	Base Load	OLSM	Percentage Improvement
Total Load (kW)	12,846.92	12,846.92	NA
Average Load (kW)	535.2883	535.2883	NA
Peak Load (kW)	821.5	689.7169	16.06% ↓
Load Factor	0.6516	0.7760	19.09% ↑
TOC Situation 1 (\$)	2624	1192	58% ↓
TOC Situation 2 (\$)	2611	1162	55.5% ↓
TOC Situation 3 (\$)	2331	1147	50.79% ↓

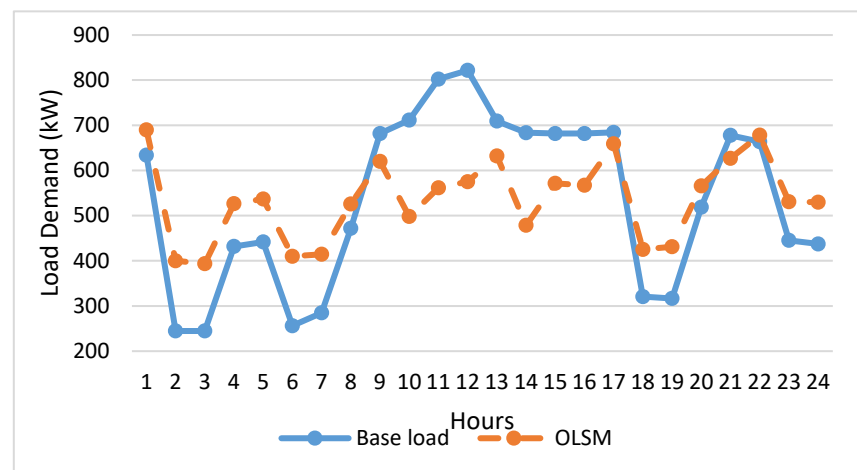


Figure 13. Modified load demand according to OLSM.

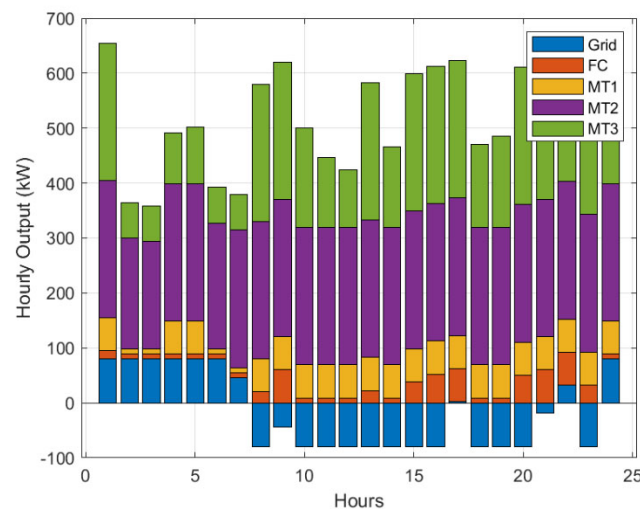


Figure 14. Hourly output of DERs for minimum TOC in Case 3, Situation 1.

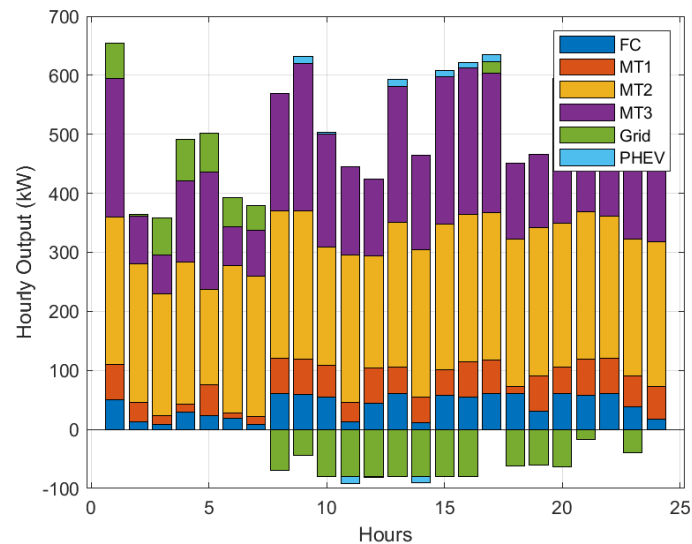


Figure 15. Hourly output of DERs for minimum TOC in Case 3, Situation 2.

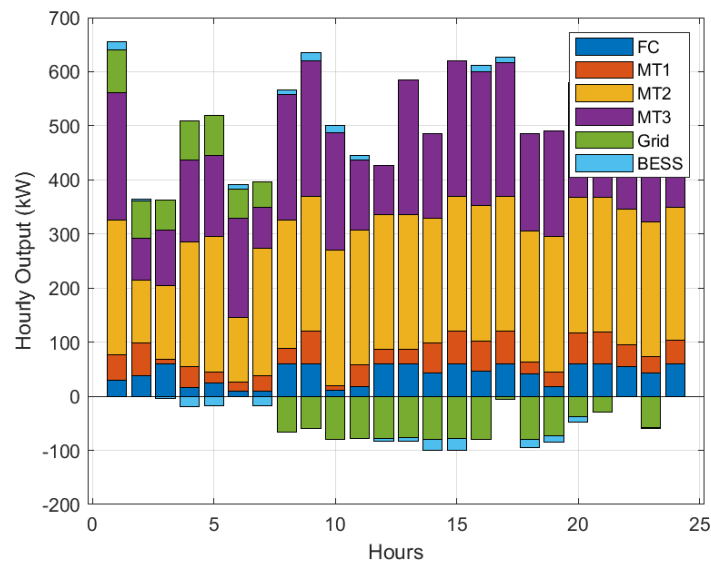


Figure 16. Hourly output of DERs for minimum TOC in Case 3, Situation 3.

The trade-off between minimum generation cost and pollutant emissions: The initial step to obtain a trade-off balance between minimum TOC and emission is to minimize the fitness function, which corresponds to the total carbon emission of the MG system which is represented by Equation (2). Upon minimizing the same using the RIME algorithm for Case 1, Situations 2 and 3, the minimum carbon emission was found to be 7555 g and 7568 g with PHEVs and with BESSs, respectively. Figures 17 and 18 represent the figures that correspond to the hourly output for DERs with minimum emissions. It can be seen that DERs with lower carbon coefficients, for example, the grid and FC, as mentioned in Table 2, are utilized to the fullest to deliver power, and hence, the grid is always positive in this case. Although there is no carbon coefficient associated with the ESS, their negative values are only to fulfill their SOC constraints.

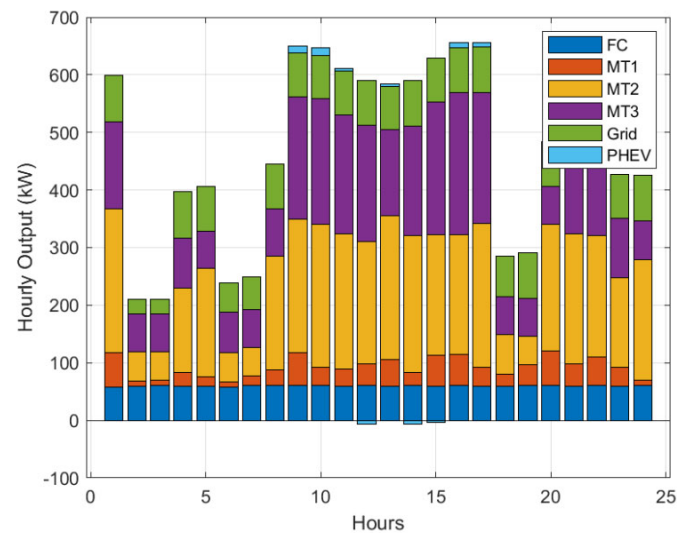


Figure 17. Hourly output of DERs for minimum emission in Case 1, Situation 2.

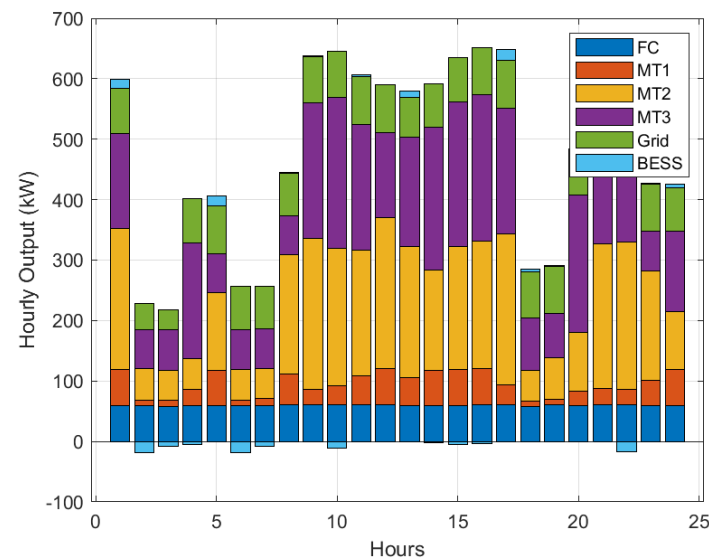


Figure 18. Hourly output of DERs for minimum emission in Case 1, Situation 3.

Thereafter, Equation (3), which is a normalized equation for minimum TOC and emission was minimized by fixing the weightage factor value at 0.5. This means that equal importance was distributed between TOC and emission while minimizing Equation (3) with the RIME algorithm. The same was done for Situations 2 and 3 and Cases 1 and 3. The results can be seen in Table 7. The balanced cost emission pair considering PHEV was (\$2793, 7694 gms) for base load and (\$1495, 7780 gms) for OLSM-based load profiles. Figure 19 depicts the hourly output of DERs when a balanced minimum cost and emissions were obtained for Situation 2, Case 3 (with PHEV for OLSM-based load). Likewise, the balanced cost emission pair considering BESSs was (\$2544, 7719 gms) for base load and (\$1556, 7790 gms) for OLSM-based load profiles. Figure 20 depicts the hourly output of DERs when a balanced minimum cost and emissions were obtained for Situation 3, Case 3 (with BESSs for OLSM-based load).

Table 7. Fitness functions evaluation using RIME for different cases and scenarios.

		Objective Function 1 (OF1)		Objective Function 2 (OF2)		Objective Function 3 (OF3)	
		Minimum Cost (\$)	Maximum Emission (gms.)	Maximum Cost (\$)	Minimum Emission (gms.)	Balanced Cost (\$)	Balanced Emission (gms.)
Situation 2 (with PHEV)	Case 1	2611	8331	4697	7555	2793	7694
	Case 3	1162	8336	4540	7549	1495	7780
Situation 3 (with BESSs)	Case 1	2331	8317	4642	7568	2544	7719
	Case 3	1147	8317	4617	7560	1556	7790

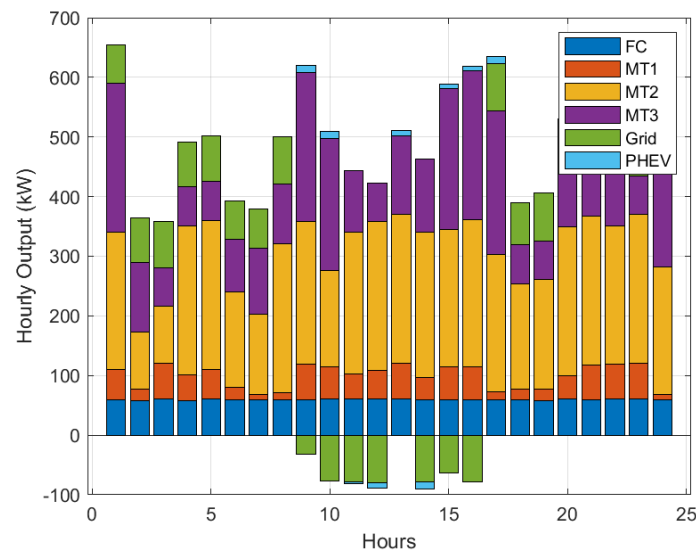


Figure 19. Hourly output of DERs for balanced cost and emission Case 3, Situation 2.

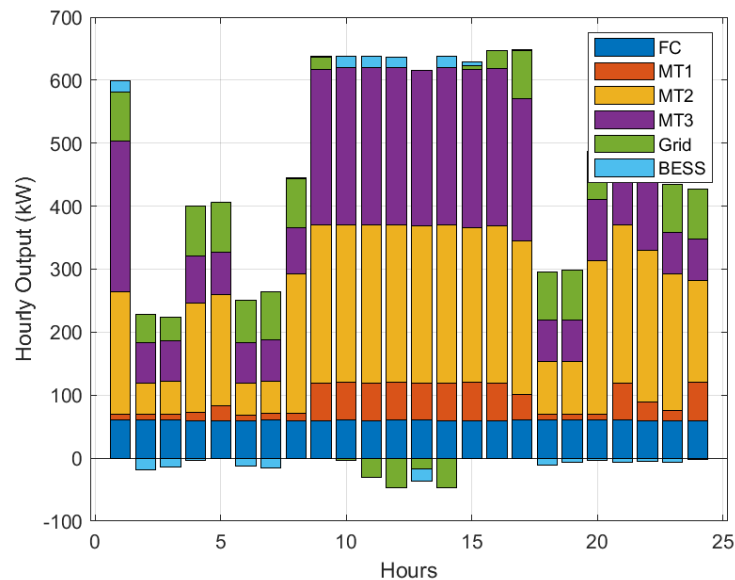


Figure 20. Hourly output of DERs for balanced cost and emission Case 3, Situation 3.

Non-parametric statistical analysis for RIME algorithm: RIME was executed 30 individual times while minimizing TOC during Case 1, Situation 1 along with five other optimization algorithms and the results were recorded with elapsed time for attaining the stopping criteria. Table 8 presents the minimum, maximum, and average values of TOC

obtained with diverse algorithms. The minimum value of standard deviation indicates the robustness of the proposed algorithm in minimum elapsed time. Figure 21 shows the convergence curve characteristics when TOC was minimized for Case 1, Situation 1. Figure 22 shows the box plot figure prepared with the statistical data from Table 8.

Table 8. Minimum, maximum, and average values of TOC obtained with diverse algorithms.

Sl No	Algorithm	Minimum (\$)	Maximum (\$)	Average (\$)	STD	Hits	Time (s)
1	RIME [33]	2624.75	2624.94	2624.77	0.032	22	3.25
2	Seagull [34]	2626.99	2633.27	2629.73	1.6573	23	3.99
3	Rat [35]	2665.43	2786.2	2718.08	29.61	25	7.66
4	Reptile Search [36]	2704.71	2957.47	2831.21	64.42	24	8.44
5	Parrot [37]	3027	3265.24	3140.62	60.22	25	8.88
6	Aquila [38]	3077.61	3347.55	3183.69	67.2003	26	9.2

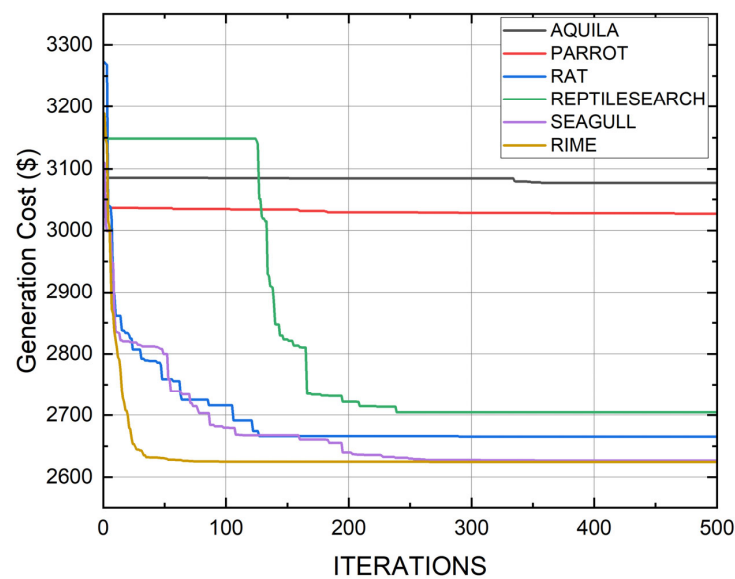


Figure 21. Convergence curve characteristics when TOC was minimized for Case 1, Situation 1.

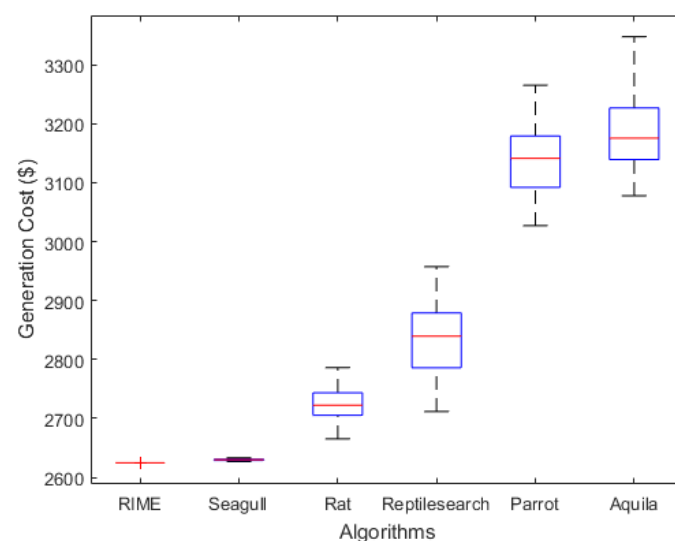


Figure 22. Box plot based on the statistical data for minimum cost of various algorithms.

5. Conclusions

The importance of energy storage systems for the cost-effective functioning of a low-voltage MG system is examined in this work. Two energy storage systems, namely BESSs and PHEVs, are involved in turns in the subject MG system. The involvement of energy storage systems reduced both the costs and the carbon emissions of the MG system since they have negligible carbon footprints. Between the two, PHEVs were involved only during their limited duration of stay in the charging station, whereas BESSs operated throughout the day. Also, PHEVs served as an additional load and relaxation in load demand during V2G and G2V operations whereas BESSs were an integral part of the MG system and operated throughout the day. Hence, cost and emission were simultaneously reduced more in the case of PHEVs than BESSs. The optimal LSM was seen to be more cost-effective than OCLSP in all the cases studied. RIME outperformed many recently developed algorithms in robustness, efficiency, and consistency for delivering better quality solutions.

Limitations of the work and future scope: Future research on microgrid systems may concentrate on many critical domains to improve their efficiency and flexibility. One approach is to tackle the uncertainty in renewable energy production by using stochastic models to reduce the unpredictability and intermittency of renewable energy sources inside the microgrid. Moreover, integrating dynamic consumer behaviors, including demand-side flexibility and incentives for load reduction, might enhance demand-side management (DSM) tactics. Creating sophisticated control algorithms to manage uncertainties in the state of charge (SOC) of plug-in hybrid electric vehicles (PHEVs), as well as their arrival and departure timings and renewable energy inputs, is a viable avenue. The concurrent use of PHEVs and battery energy storage systems (BESSs) as hybrid storage solutions may be investigated to optimize storage capacity and operating efficiency. Moreover, the implementation of load-curtailling policies and the evaluation of their efficacy against current load-shifting procedures might reveal the most economical and consumer-oriented demand-side management methods. Ultimately, including traditional distribution network restrictions, voltage profiles, and power quality metrics would enhance the relevance of these results to real-world situations, therefore reconciling theoretical models with actual microgrid management.

Author Contributions: Conceptualization, B.D. and S.K.; methodology, B.D.; software, B.D.; validation, B.D., N.F. and M.R.; formal analysis, P.M.; investigation, N.F.; resources, S.K.; data curation, S.K.; writing—original draft preparation, B.D. Proofreading and approval, S.K. All authors have read and agreed to the published version of the manuscript.

Funding: This research was partly funded by the South African National Energy Development Institute, SANEDI JET Project RFQ0622, NRF Thuthuka Grant Number 138177, and the Eskom Tertiary Education Support Programme (TESP), South Africa.

Data Availability Statement: The raw data underlying this article will be made available to readers on request.

Acknowledgments: The authors gratefully acknowledge the SANEDI JET DSM Project Bid0622 and Center for Intelligent Systems and Emerging Technologies at Cape Peninsula University of Technology, South Africa, for the facilities provided to do this work. The authors wish to thank the reputed reviewers whose valuable inputs helped them elevate the standard of the manuscript. The authors also extend their acknowledgment to Srikant Misra, GIET University, Gunupur, Odisha, India for his generous Contribution toward the final version of the manuscript.

Conflicts of Interest: The authors declare that they have no conflicts of interest.

List of Abbreviations

<i>BESSs</i>	Battery energy storage systems
<i>PHEV</i>	Plug-in Hybrid Electric Vehicles
<i>OSLM</i>	Optimal Load-shifting Method
<i>TOC</i>	Total Operating Cost
<i>OCLSP</i>	Order Characteristics Load-shifting Policy
<i>DG</i>	Distributed Generation
<i>EMS</i>	Energy Management Systems
<i>MG</i>	Microgrids
<i>CPN</i>	Coloured Petri Nets
<i>HMg</i>	Hybrid Microgrid
<i>LV</i>	Low Voltage
<i>DER</i>	Distributed Energy Sources
<i>DSM</i>	Demand-Side Management
<i>BSS</i>	Battery Storage System
<i>GES</i>	Generalized Energy Storage
<i>SMA</i>	Slime Mould Algorithm
<i>EV</i>	Electric Vehicles
<i>SDG</i>	Solar Distributed Generations
<i>BES</i>	Battery Energy Storages
<i>PFCS</i>	Public Fast-Charging Stations
<i>EVCS</i>	Electric Vehicle Charging Stations
<i>ESS</i>	Energy Storage Systems
<i>TOU</i>	Time of use

Appendix A

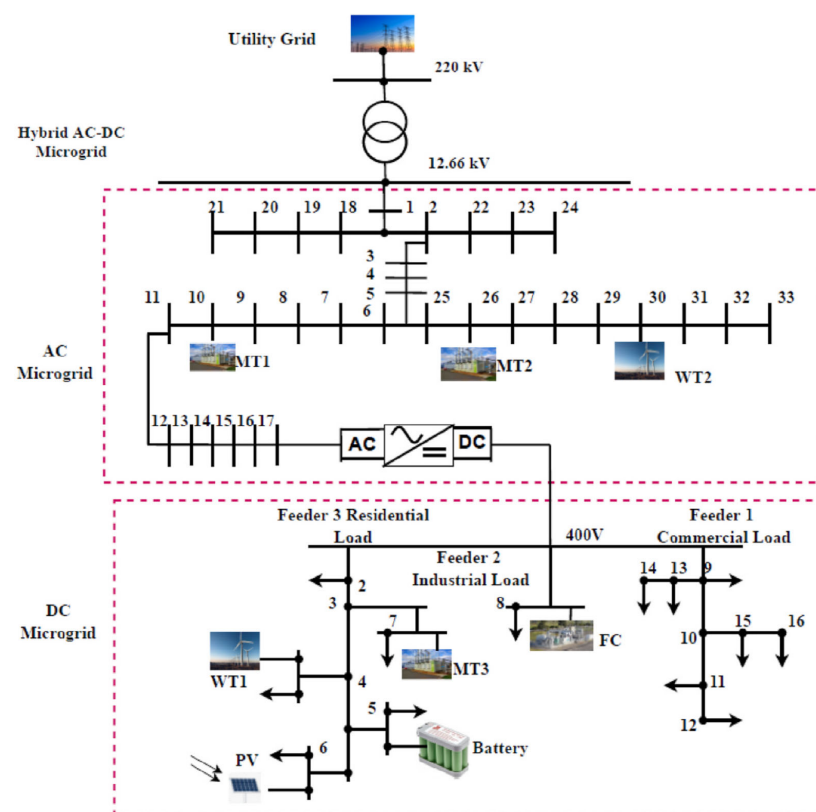


Figure A1. Subject AC/DC Microgrid [25].

References

1. Wang, L.; An, X.; Xu, H.; Zhang, Y. Multi-agent-based collaborative regulation optimization for microgrid economic dispatch under a time-based price mechanism. *Electr. Power Syst. Res.* **2022**, *213*, 108760. [[CrossRef](#)]
2. Zhou, Y.; Xia, Z.; Liu, X.; Deng, Z.; Fu, X.; Kupecki, J.; Jin, B.; Li, X. Online energy management optimization of hybrid energy storage microgrid with reversible solid oxide cell: A model-based study. *J. Clean. Prod.* **2023**, *423*, 138663. [[CrossRef](#)]
3. Shi, Z.; Zhang, T.; Liu, Y.; Feng, Y.; Wang, R.; Huang, S. Optimal design and operation of islanded multi-microgrid system with distributionally robust optimization. *Electr. Power Syst. Res.* **2023**, *221*, 109437. [[CrossRef](#)]
4. Grisales-Noreña, L.F.; Ocampo-Toro, J.A.; Montoya-Giraldo, O.D.; Montano, J.; Hernández, J.C. Optimal operation of battery storage systems in standalone and grid-connected DC microgrids using parallel metaheuristic optimization algorithms. *J. Energy Storage* **2023**, *65*, 107240. [[CrossRef](#)]
5. Basak, S.; Bhattacharyya, B. Optimal scheduling in demand-side management based grid-connected microgrid system by hybrid optimization approach considering diverse wind profiles. *ISA Trans.* **2023**, *139*, 357–375. [[CrossRef](#)]
6. Tukkee, A.S.; Wahab, N.I.B.A.; Mailah, N.F.B. Optimal sizing of autonomous hybrid microgrids with economic analysis using grey wolf optimizer technique. *e-Prime-Adv. Electr. Eng. Electron. Energy* **2023**, *3*, 100123. [[CrossRef](#)]
7. Liu, X.M.; Zhao, M.; Wei, Z.H.; Lu, M. The energy management and economic optimization scheduling of microgrid based on Colored Petri net and Quantum-PSO algorithm. *Sustain. Energy Technol. Assess.* **2022**, *53*, 102670. [[CrossRef](#)]
8. Nwulu, N.I.; Xia, X. Optimal dispatch for a microgrid incorporating renewables and demand response. *Renew. Energy* **2017**, *101*, 16–28. [[CrossRef](#)]
9. Misra, S.; Dey, B.; Panigrahi, P.K.; Ghosh, S. A Swarm-Intelligent based Load-Shifting Strategy for Clean and Economic Microgrid Operation. *ISA Trans.* **2024**, *147*, 265–287. [[CrossRef](#)] [[PubMed](#)]
10. Misra, S.; Panigrahi, P.K.; Ghosh, S.; Dey, B. Economic operation of a microgrid system with renewables considering load shifting policy. *Int. J. Environ. Sci. Technol.* **2023**, *21*, 1–14. [[CrossRef](#)]
11. Chakraborty, A.; Ray, S. Operational cost minimization of a microgrid with optimum battery energy storage system and plug-in-hybrid electric vehicle charging impact using slime mould algorithm. *Energy* **2023**, *278*, 127842. [[CrossRef](#)]
12. Datta, J.; Das, D. Energy management study of interconnected microgrids considering pricing strategy under the stochastic impacts of correlated renewables. *IEEE Syst. J.* **2022**, *17*, 3771–3782. [[CrossRef](#)]
13. Chakraborty, A.; Ray, S. Minimizing Operational Cost of a Microgrid with an Optimum Storage System Size and PHEV Charging Demand. In Proceedings of the 2024 IEEE 9th International Conference for Convergence in Technology (I2CT), Pune, India, 5–7 April 2024; pp. 1–7.
14. Shi, Z.; Zhang, T.; Liu, Y.; Feng, Y.; Wang, R.; Huang, S. Energy management of multi-microgrid system with renewable energy using data-driven distributionally robust optimization. *Int. J. Green Energy* **2024**, *21*, 2699–2711. [[CrossRef](#)]
15. Zhou, Y.; Wang, J.; Yang, M.; Xu, H. Hybrid active and passive strategies for chance-constrained bilevel scheduling of community multi-energy system considering demand-side management and consumer psychology. *Appl. Energy* **2023**, *349*, 121646. [[CrossRef](#)]
16. Chakraborty, A.; Ray, S. Multi-objective operational cost management with minimum net emission of a smart microgrid. *Electr. Power Compon. Syst.* **2024**, *52*, 1870–1891. [[CrossRef](#)]
17. Yang, J.; Xu, W.; Ma, K.; Chen, J.; Guo, W. Integrated demand-side management for multi-energy system based on non-cooperative game and multi-energy pricing. *Sustain. Energy Grids Netw.* **2023**, *34*, 101047. [[CrossRef](#)]
18. Li, Y.; Wang, J.; Zhou, Y.; Wei, C.; Guan, Z.; Chen, H. Multi-dimension day-ahead scheduling optimization of a community-scale solar-driven CCHP system with demand-side management. *Renew. Sustain. Energy Rev.* **2023**, *185*, 113654. [[CrossRef](#)]
19. Sharma, A.K.; Saxena, A.; Palwalia, D.K. Oppositional Slime Mould Algorithm: Development and application for designing demand side management controller. *Expert Syst. Appl.* **2023**, *214*, 119002. [[CrossRef](#)]
20. Nodehi, M.; Zafari, A.; Radmehr, M. A new energy management scheme for electric vehicles microgrids concerning demand response and reduced emission. *Sustain. Energy Grids Netw.* **2022**, *32*, 100927. [[CrossRef](#)]
21. Blazek, V.; Vantuch, T.; Slanina, Z.; Vysocky, J.; Prokop, L.; Misak, S.; Piecha, M.; Walendziuk, W. A novel approach to utilization vehicle to grid technology in microgrid environment. *Int. J. Electr. Power Energy Syst.* **2024**, *158*, 109921. [[CrossRef](#)]
22. Pal, A.; Bhattacharya, A.; Chakraborty, A.K. Placement of public fast-charging station and solar distributed generation with battery energy storage in distribution network considering uncertainties and traffic congestion. *J. Energy Storage* **2021**, *2021*, 41, 102939. [[CrossRef](#)]
23. Pal, A.; Bhattacharya, A.; Chakraborty, A.K. Allocation of electric vehicle charging station considering uncertainties. *Sustain. Energy Grids Netw.* **2021**, *25*, 100422. [[CrossRef](#)]
24. Pal, A.; Bhattacharya, A.; Chakraborty, A.K. Planning of EV charging station with distribution network expansion considering traffic congestion and uncertainties. *IEEE Trans. Ind. Appl.* **2023**, *59*, 3810–3825. [[CrossRef](#)]
25. Krishna, R.; Hemamalini, S. Improved TLBO algorithm for optimal energy management in a hybrid microgrid with support vector machine-based forecasting of uncertain parameters. *Results Eng.* **2024**, *24*, 102992. [[CrossRef](#)]

26. Alghamdi, A.S. Microgrid energy management and scheduling utilizing energy storage and exchange incorporating improved gradient-based optimizer. *J. Energy Storage* **2024**, *97*, 112775. [[CrossRef](#)]
27. Dey, B.; Sharma, G.; Bokoro, P.N. Economic management of microgrid using flexible non-linear load models based on price-based demand response strategies. *Results Eng.* **2024**, *24*, 102993. [[CrossRef](#)]
28. Dey, B.; Misra, S.; Chhualsingh, T.; Sahoo, A.K.; Singh, A.R. A hybrid metaheuristic approach to solve grid centric cleaner economic energy management of microgrid systems. *J. Clean. Prod.* **2024**, *448*, 141311. [[CrossRef](#)]
29. Sharma, S.; Bhattacharjee, S.; Bhattacharya, A. Probabilistic operation cost minimization of Micro-Grid. *Energy* **2018**, *148*, 1116–1139. [[CrossRef](#)]
30. Chakraborty, A.; Ray, S. Microgrid operational energy management with plug-in hybrid electric vehicles charging demand. *Electr. Eng.* **2024**, *106*, 2245–2263. [[CrossRef](#)]
31. Datta, J.; Das, D. Energy management of multi-microgrids with renewables and electric vehicles considering price-elasticity based demand response: A bi-level hybrid optimization approach. *Sustain. Cities Soc.* **2023**, *99*, 104908. [[CrossRef](#)]
32. Misra, S.; Panigrahi, P.K.; Ghosh, S.; Dey, B. A metaheuristic approach to compare different combined economic emission dispatch methods involving load shifting policy. *Environ. Dev. Sustain.* **2024**, 1–23. [[CrossRef](#)]
33. Su, H.; Zhao, D.; Heidari, A.A.; Liu, L.; Zhang, X.; Mafarja, M.; Chen, H. RIME: A physics-based optimisation. *Neurocomputing* **2023**, *532*, 183–214. [[CrossRef](#)]
34. Dhiman, G.; Kumar, V. Seagull optimization algorithm: Theory and its applications for large-scale industrial engineering problems. *Knowl. -Based Syst.* **2019**, *165*, 169–196. [[CrossRef](#)]
35. Dhiman, G.; Garg, M.; Nagar, A.; Kumar, V.; Dehghani, M. A novel algorithm for global optimization: Rat Swarm Optimizer. *J. Ambient Intell. Human. Comput.* **2021**, *12*, 8457–8482. [[CrossRef](#)]
36. Abualigah, L.; Elaziz, M.A.; Sumari, P.; Geem, Z.W.; Gandomi, A.H. Reptile Search Algorithm (RSA): A nature-inspired meta-heuristic optimizer. *Expert Syst. Appl.* **2022**, *191*, 116158. [[CrossRef](#)]
37. Lian, J.; Hui, G.; Ma, L.; Zhu, T.; Wu, X.; Heidari, A.A.; Chen, Y.; Chen, H. Parrot optimizer: Algorithm and applications to medical problems. *Comput. Biol. Med.* **2024**, *172*, 108064. [[CrossRef](#)]
38. Abualigah, L.; Yousri, D.; Elaziz, M.A.; Ewees, A.A.; Al-Qaness, M.A.A.; Gandomi, A.H. Aquila optimizer: A novel meta-heuristic optimization algorithm. *Comput. Ind. Eng.* **2021**, *157*, 107250. [[CrossRef](#)]

Disclaimer/Publisher’s Note: The statements, opinions and data contained in all publications are solely those of the individual author(s) and contributor(s) and not of MDPI and/or the editor(s). MDPI and/or the editor(s) disclaim responsibility for any injury to people or property resulting from any ideas, methods, instructions or products referred to in the content.